Available online at www.sciencedirect.com
SCIENCE DIRECT®
Journal of Theoretical Biology 232 (2005) 569–585
Journal of Theoretical Biology
www.elsevier.com/locate/yjtbi

Model of coupled transient changes of Rac, Rho, adhesions and stress fibers alignment in endothelial cells responding to shear stress

G. Civelekoglu-Scholey[a,b], A. Wayne Orr[c], I. Novak[d], J.-J. Meister[a], M.A. Schwartz[e], A. Mogilner[b,f,*]

[a]*Laboratory of Cell Biophysics, Swiss Federal Institute of Technology, Lausanne, Switzerland*
[b]*Laboratory of Cell and Computational Biology, Center for Genetics and Development, University of California, Davis, CA 95616, USA*
[c]*Cardiovascular Research Center, University of Virginia, Charlottesville, VA 22908, USA*
[d]*Center for Cell Analysis and Modeling, University of Connecticut Health Center, Farmington, CT 06030, USA*
[e]*Departments of Biomedical Engineering and Microbiology, University of Virginia, Charlottesville, VA 22908, USA*
[f]*Department of Mathematics, University of California, One Shield Avenue, Davis, CA 95616-8633, USA*

Received 27 November 2003; received in revised form 17 July 2004; accepted 15 September 2004

Abstract

Interactions of cell adhesions, Rho GTPases and actin in the endothelial cells' response to external forces are complex and not fully understood, but a qualitative understanding of the mechanosensory response begins to emerge. Here, we formulate a mathematical model of the coupled dynamics of cell adhesions, small GTPases Rac and Rho and actin stress fibers guiding a directional reorganization of the actin cytoskeleton. The model is based on the assumptions that the interconnected cytoskeleton transfers the shear force to the adhesion sites, which in turn transduce the force into a chemical signal that activates integrins at the basal surface of the cell. Subsequently, activated and ligated integrins signal and transiently de-activate Rho, causing the disassembly of actin stress fibers and inhibiting the maturation of focal complexes into focal contacts. Focal complexes and ligated integrins activate Rac, which in turn enhances focal complex assembly. When Rho activity recovers, stress fibers re-assemble and promote the maturation of focal complexes into focal contacts. Merging stress fibers self-align, while the elevated level of Rac activity at the downstream edge of the cell is translated into an alignment of the cells and the newly forming stress fibers in the flow direction. Numerical solutions of the model equations predict transient changes in Rac and Rho that compare well with published experimental results. We report quantitative data on early alignment of the stress fibers and its dependence on cell shape that agrees with the model.

Keywords: Endothelial cells; Focal adhesion; Rho GTPases; Stress fibers; Mathematical model

1. Introduction

The endothelial cell monolayer lining the inner wall of the vascular system is exposed to forces produced by blood flow, including fluid shear stress, and the cyclic circumferential stretch caused by the cardiac cycle (Girard and Nerem, 1993; Davies, 1995). Before exposure to shear stress, endothelial cells have a polygonal shape, actin filaments are organized in a dense isotropic peripheral band underlying the cell membrane and in bundles distributed randomly throughout the cell. Sites where the cells adhere to the surface are randomly distributed around the cell periphery. Simulation of blood flow in experimental models reveals that endothelial cells respond to the onset of the flow by changes in intracellular ionic flux, signaling events, gene regulation, transcription and translation that occur on a hierarchy of time scales,

*Corresponding author. Tel.: +1 530 752 1072; fax: +1 530 752 6635.
E-mail address: mogilner@math.ucdavis.edu (A. Mogilner).

0022-5193/$ - see front matter © 2004 Elsevier Ltd. All rights reserved.
doi:10.1016/j.jtbi.2004.09.004

from seconds to hours (Davies, 1995). The cell membrane, intercellular junctions and three major cytoskeletal systems—microtubules, actin and intermediate filaments—also re-organize drastically (Galbraith et al., 1998). Here, we focus exclusively on the actin cytoskeleton response which is the most prominent in early stages, and do not explicitly discuss the involvement of cell membrane, cell–cell junctions, microtubules and intermediate filaments in this response.

Following the onset of the flow, the dense peripheral band of actin filaments partially dissolves, and the filaments rearrange to create bundles that are referred to as stress fibers aligned along the flow direction (Davies, 1995). The anchorage sites where the cell adheres to the substrate elongate in the flow direction, and new adhesion sites appear preferentially at the down-stream edge of the cell (Davies et al., 1994; Mathur et al., 2000). In later stages, the adhesion sites mature into stable structures that cluster in large aggregates at the end of the stress fibers that run the length of the cell, and the cell assumes an elongated shape with its main axis aligned in the direction of its stress fibers. Cytoskeletal alignment is an important adaptive process leading to the reduction of the mechanical load (Girard and Nerem, 1993; Davies, 1995).

In this paper, we develop two models of coupled dynamics of actin stress fibers, adhesions, Rac and Rho, and examine the models mathematically. In the rest of this section, we briefly review these coupled dynamics. In Section 2, we describe the relevant data on responses of the endothelial cells to the shear flow and formulate qualitative models of the temporal and angular aspects of the phenomenon. We translate the models of temporal response and of stress fibers' alignment into sets of mathematical equations in Sections 3 and 4, respectively. We report results of mathematical analyses and computer simulations in Sections 5 and 6. We discuss the model's implications for cell physiology in Section 7.

Our models, in addition to the data reported below and data of (Tzima et al., 2001, 2002; Zimerman, 2004), were inspired by the diagram of the possible feedback loops controlling the formation and growth of focal contacts suggested in Fig. 4 of Geiger and Bershadsky (2001). A different semi-quantitative model of the relevant signal transduction pathways, based on the idea that an integration between the rapid events stimulated by shear stress and the longer term events is mediated by tyrosine kinases that serve to regulate these multiple pathways was proposed in Ishida et al. (1997). Purely mechanical alignment of the actin cytoskeleton (rather than its disassembly and assembly de novo at new locations and directions regulated by biochemical signals) was modeled in Sherratt and Lewis (1993) and Suciu et al. (1997).

1.1. Actin cytoskeleton and adhesion sites

Actin network and bundles of parallel actin filaments called *stress fibers* are interconnected across the cell (Bray, 2001; Wang et al., 1993; Maniotis et al., 1997). The length of the stress fibers is comparable to the cell size (Mathur et al., 2000), so the cell is able to use sliding of myosin and actin bundles to generate global contractile forces. Stress fibers turn over rapidly, within minutes (McGrath et al., 1998; Davies, 1995). Stress fibers terminate both on the basal and apical surfaces of the cell (Kano et al., 2000) as well as on intercellular junctions (Zhao et al., 1995) and nucleus (Fig. 1A). On the basal surface, stress fibers terminate at *focal*

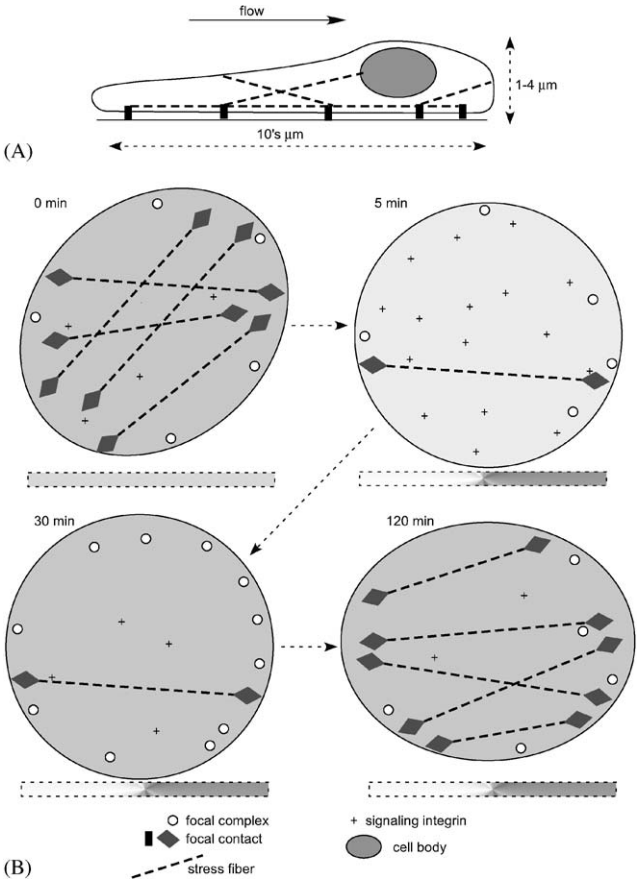

Fig. 1. A. Schematic side view of the cell sheared by the flow. B. Sequence of events leading to the cytoskeletal alignment in response to fluid flow (view from above). Initially, the stress fibers are aligned with the cell long axis, and the cell is oriented randomly. A few minutes following the onset of the flow, the number of ligated signaling integrins increases, the activated Rho concentration (shading) decreases, the stress fibers disassemble, and the activated Rac concentration (shading of the bar below the cell) increases in a polarized manner, such that there is elevated levels of Rac at the downstream edge of the cell. In a few tens of minutes, the ligated integrins cease signaling and Rho concentration increases back to its baseline level. Eventually, in two hours, Rac concentration returns to baseline, and focal complexes mature into focal contacts. Simultaneously, the cell long axis reorient in the direction of the flow, and the stress fibers reassemble and align with the cell new long axis.

adhesions that are mostly located at the cell periphery (Girard and Nerem, 1993).

Transmembrane receptors, *integrins*, are a key component of the dynamic *adhesion* complexes that physically connect the external surface to the cytoskeleton. Their short cytoplasmic domains associated with adaptor proteins connect the integrins to the cytoskeleton and to signaling proteins (Giancotti and Ruoslahti, 1999). Adhesion complexes show significant diversity (Zamir and Geiger, 2001). *Focal contacts* are complex multimolecular assemblies containing hundreds to thousand of integrins (Schwartz and Shattil, 2000) that are enriched in vinculin, paxillin and many other proteins (Zamir and Geiger, 2001). The integrins exchange rapidly, on a time scale of a few minutes. Besides adaptor proteins, several types of signaling molecules, including tyrosine kinases and phosphatases are components of focal contacts. Most focal contacts grow out of small *focal complexes* (Zamir and Geiger, 2001) that contain many, but not all, of the protein components of focal contacts.

Adhesions are important sites of signal transduction propagating signals arising from the integrins following their engagement with the substratum (Davies et al., 1994). Involvement of integrins in the mechanosensing process was first proposed in Wang et al. (1993), and was later confirmed by discoveries of many intracellular signaling pathways activated by integrin mediated adhesion (Giancotti and Ruoslahti, 1999; Schoenwaelder and Burridge, 1999) that regulate cytoskeletal dynamics. Integrins signal through the cell membrane in both directions (Schoenwaelder and Burridge, 1999): ligand binding to integrins transmit signals that initiate rearrangements of the actin cytoskeleton, while signals from the cell affect integrins clustering and affinity for their ligands.

One of the important questions is how the shear stress at the luminal cell surface is transmitted to the adhesion sites at the basal surface. The existence of a molecular sensor at the luminal surface sending a diffusible chemical signal to the basal surface cannot be ruled out, however, a growing body of data supports another possibility: Due to the mechanical integrity and global stiffness of the cytoskeleton, physiological shear stress cannot deform the cytoskeleton (Appendix A.1), and therefore the cytoskeletal scaffold withstanding the shear forces transduces the stress mechanically from the luminal surface to the adhesions at the basal surface (Mathur et al., 2000).

Force is known to regulate the assembly and turnover of adhesions (Davies et al., 1994; Zamir and Geiger, 2001). Tension 'reinforces' focal adhesions in seconds (Balaban et al., 2001; Riveline et al., 2001) and triggers their elongation in the direction of the force (Balaban et al., 2001). The exact mechanism of force-regulated adhesion turnover is not known, however, data indicate that force application to integrins leads to conformational activation of signaling molecules associated with nascent adhesions and promotes recruitment of proteins typical of focal contacts, such as paxillin and vinculin, leading to reinforcement and maturation of these adhesions (Zamir and Geiger, 2001; Sawada and Sheetz, 2002; von Wichert et al., 2003; Geiger and Bershadsky, 2001).

1.2. Relationship between Rho GTPases, actin cytoskeleton and focal adhesions

In this paper, we focus on **Rho** and **Rac** mediated pathways regulating the remodeling of actin cytoskeleton and focal adhesions (Tzima et al., 2001, 2002). The small G-proteins Rho and Rac regulate a wide variety of cell functions (Hall, 1998; Ridley, 2001) operating through a host of effectors that interact with the GTP-bound proteins. A variety of cytokines induces loading of Rho and Rac that stay in the cytosol in GDP-bound form with GTP. Activated GTPases translocate to their functioning sites at specific subcellular compartments.

Activation of Rho is required for the formation of focal contacts and associated stress fibers, whereas formation of focal complexes depends on the activity of Rac (Geiger and Bershadsky, 2001). Rho induces formation of focal contacts by activation of both ROCK- and mDia1-dependent pathways. The main function of the ROCK-dependent pathway is to phosphorylate myosin light chain kinase, activating myosin driven cell contractility. The resulting increase in tension force at focal complexes triggers the transition of these structures into focal contacts (Rottner et al., 1999; Geiger and Bershadsky, 2001; Webb et al., 2002). Rac activates and drives the formation of focal complexes (Rottner et al., 1999; Webb et al., 2002) possibly by promoting the assembly of isotropic actin networks that serve as scaffolds for focal complex growth (Geiger and Bershadsky, 2001). Furthermore, there could be an additional pathway from Rho GTPases to adhesions through clustering of ligated integrins within focal complexes that requires Rac, and within focal adhesions that requires Rho (Schwartz and Shattil, 2000). Integrins, Rac and Rho are intimately connected on multiple levels, and it is possible that successive waves of integrin–Rac–Rho-dependent signals regulate cytoskeleton and adhesions according to a complex spatio-temporal pattern (Schwartz and Shattil, 2000).

General mechanisms of the crosstalk between Rho and Rac have been elucidated though many specific questions remain unanswered. Rho- and Rac-induced phenotypes seem to be mutually exclusive: expression of active Rac renders neuronal cells refractory to Rho-induced signaling (Van Leeuwen et al., 2003). Similarly, inhibition of the Rho pathway induces Rac-associated

phenotypes and, vice versa, inhibition of Rac signaling promotes Rho-related phenotypes (Arthur and Burridge, 2001). Rac induces rapid and transient inactivation of Rho (Nimnual et al., 2003). Rho- and Rac-mediated pathways also regulate each other in a more complex way on multiple time scales (Rottner et al., 1999).

Similarly, signaling pathways by which integrins regulate Rac and Rho are not well characterized. Formation of new integrin–ligand connections activates a cascade of signaling events including phosphorylation of kinases, which regulate Rac and Rho activities (Schwartz and Shattil, 2000). Specifically, ligated integrins and focal complexes activate Rac (Schwartz and Shattil, 2000; Zamir et al., 2000) and transiently suppress Rho GTP loading (Arthur et al., 2000). Additional cell-surface receptors can cooperate with integrins in the adaptation of Rho activity (Schwartz and Shattil, 2000).

2. Relevant data and models of mechanosensory response to shear stress

Recent studies have led to a new understanding of signaling and actin reorganization induced by shear stress (Tzima et al., 2001, 2002) and of stress fibers dynamics (Zimerman, 2004; our data). In this section, we first describe the relevant data, and then formulate qualitative models of the temporal mechanosensory response and stress fibers' alignment.

2.1. Temporal dynamics of stress fibers, Rac, Rho and focal complexes and contacts (Fig. 1) (Tzima et al., 2001, 2002)

De novo integrin–ligand binding is detectable 2 min after the onset of the flow. There is no indication that this integrin activation has any polarity. Downstream to and induced by new integrin–ligand binding, the activated Rho concentration decreases by about 50% in 5 min. This brief and transient Rho inhibition is followed by a slower (tens of minutes) restoration phase when the activated Rho concentration returns to baseline. The time course of the biphasic regulation of Rho corresponds to the disassembly of existent stress fibers followed by the assembly of new ones. Following the exposure to shear stress, Rac activity undergoes a transient increase to three times its initial level within 30 min. Similar to Rho downregulation, Rac activation is also found to be downstream to de novo integrin ligation. Subsequent to the transient increase, the total Rac activity returns back to its baseline level within few tens of minutes.

2.2. Spatial dynamics of Rac and the alignment of the cells and stress fibers (Tzima et al., 2001, 2002; our new experimental observations (Fig. 2))

The transient Rac increase is localized primarily to the downstream edge of the cell. When the average level of activated Rac returns to the baseline, it remains directional (Fig. 1). Experiments using dominant inhibitory mutants of Rac show that this Rac gradient is not required for global changes in the actin cytoskeleton (the disassembly of existent stress fibers followed by the assembly of new ones), but is essential for the orientation of newly forming stress fibers in the flow direction.

In order to quantify the alignment of the cell and its stress fibers, we observed the effect of the shear flow on the actin distribution in more than 240 cells (Fig. 2, Table 1). Actin was stained with Alexa-488 phalloidin (Molecular Probes), and the cells were left untreated (125 cells) or exposed to shear for 60 min (115 cells). (This is the earliest time point for which any alignment can be detected. Note that full alignment takes about 16 h. A detailed description of this experiment can be found in Tzima et al. (2001, 2002).) Accompanying images where the cells were stained with an antibody to

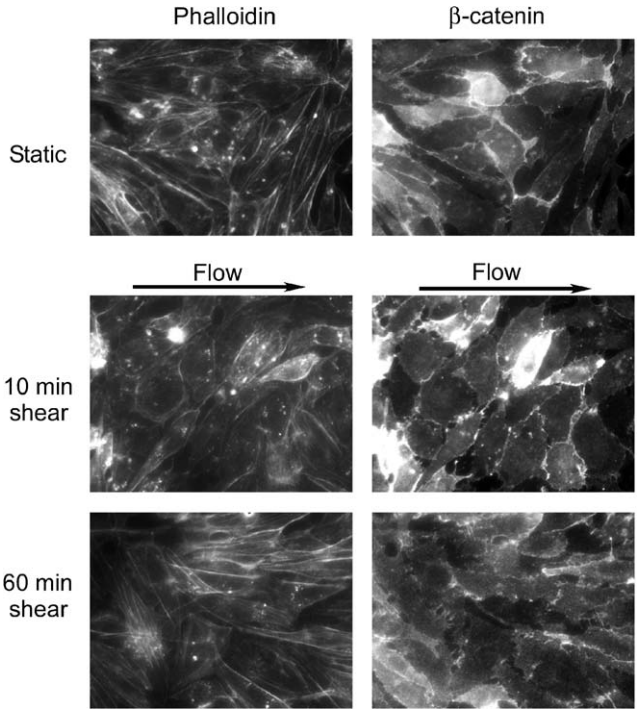

Fig. 2. Time course of F-actin organization and cell shape changes. Cells were subjected to shear stress, fixed and stained with Alexa-488 phalloidin (left) to detect actin stress fibers and with antibody to β-catenin (right) to show cell borders (see Materials and Methods in (Tzima et al., 2001)). Both before and after the flow, the stress fibers align with the cells' long axes. The long axes of the cells orient along the flow (quantitative data based on these images is reported in Table 1).

Table 1
Stress fibers' orientation (average ± standard deviation)

L/H	<0.4	0.4 to 0.8	0.8 to 1.2	1.2 to 1.6	<1.6
Static ($n = 125$)	76.3 ± 8.3 ($n = 3$)	55.8 ± 17.4 ($n = 56$)	38.2 ± 17.8 ($n = 30$)	29.5 ± 15.0 ($n = 21$)	18.5 ± 14.1 ($n = 15$)
1 h Shear ($n = 115$)	79.0 ± 7.9 ($n = 3$)	57.7 ± 18.0 ($n = 31$)	37.3 ± 15.3 ($n = 25$)	24.2 ± 14.2 ($n = 31$)	13.8 ± 10.8 ($n = 25$)

β-catenin, a protein that binds to the cytoplasmic domain of cadherins and is a marker for cell–cell junctions, showed cell boundaries (Fig. 2). We used micrographs like those in Fig. 2 to (i) analyse cells' dimensions parallel and perpendicular to flow direction with Image J software, (ii) determine, by eye, the predominant direction of the stress fibers in each cell, and (iii) measure the average orientation of the stress fibers relative to the direction of flow with a protractor. (Visual observations and the use of the protractor in this case proved to be simpler than and as effective as some automated image processing techniques.) The results are reported in Table 1. In this table, we classify the cells by the calculated ratio (L/H), where "L = length" and "H = height" are the distances across the cell parallel and perpendicular to the direction of shear, respectively. So, cells with low ratios are aligned perpendicular to the flow direction, and those with high ratios are aligned parallel to the flow direction. Parameter n shows the numbers of the cells observed in each class. In Table 1, we also report the average orientation of the stress fibers relative to the flow direction in each together with the standard deviations.

Our data indicates that in the first hour after the onset of flow the cells start to align in the direction of the flow: the number of the cells aligned perpendicular to the flow direction decreases, while the number of the cells aligned parallel to the flow direction increases (Table 1). The orientation of the stress fibers in elongated cells is, on average, along the long axis of the cell, independently of whether the cell's long axis itself is aligned in the flow direction or not (Table 1). Visual observations (that are hard to quantify, because the cell shape is irregular) of the micrographs as in Fig. 2 also confirm that, in individual cells, the stress fibers are highly aligned with each other and oriented along the cell's long axis. The stress fibers are also aligned with each other in the cells that are not elongated; in this case the average stress fiber orientation does not correlate with the flow direction.

2.3. Coupled dynamics of adhesions and stress fibers (Zimerman et al., 2004)

Stress fiber assembly dynamics were described in detail recently in spreading fibroblasts (Zimerman, 2004). (The corresponding dynamics in endothelial cells is very likely to be similar.) First, small adhesion structures with an F-actin core emerged and rapidly (minutes) matured to adhesion "doublets" interconnected by short actin bundles. Then, long actin bundles were formed over tens of minutes by lining up and "fusion" of shorter bundles. Finally, over a few hours, the long bundles matured into stress fibers stretching across the whole cell with focal adhesions at the cell periphery associated with the fibers' ends. The actin bundles were highly dynamic undergoing translocation, shortening, splitting and convergence.

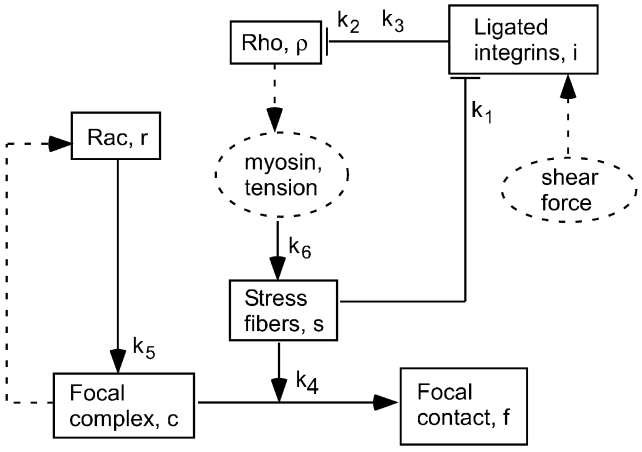

Fig. 3. Illustration of the positive (arrows) and negative (lines with bars at their end) feedbacks in the model. The model variables are in rectangular boxes; important implicit factors are in oval boxes. The dashed and solid lines show the 'fast' and 'slow' interactions, respectively. Model parameters (reaction rates) are shown near the arrows/lines for the corresponding reactions (see equations in Section 3).

2.4. Qualitative model of the temporal mechanosensory response (Fig. 3)

Here, we propose a model of a few crucial mechanochemical feedbacks underlying the cell response to shear flow, which allows us to examine the phenomenon quantitatively. The temporal dynamics of the model is summarized in Fig. 3. This model is in general agreement with the qualitative scheme suggested in Geiger and Bershadsky (2001). We assume that the interconnected cytoskeleton withstands the shear applied at the luminal surface and transmits it mechanically to the basal surface and to cell–cell contacts, where stress is applied to the existent cell adhesions. This external stress adds on to the existent myosin generated

internal tension at the focal contacts and cell–cell adhesions, exceeding a threshold at which a conformational transition triggering a diffusible signal (probably involving c-Src and/or PIP_3) occurs. This signal globally activates integrins at the basal surface leading to their ligation. The ligated integrins, in turn, generate a signal inactivating Rho. One of the main assumptions of the model is that the Rho inhibition decays with time. One possibility is that this effect is due to a changed tension applied to the ligated integrins, when decreased level of Rho causes stress fibers disintegration and relative increase of the external force vs internal myosin tension. Another possibility—that there exists an inhibitory adaptor protein that binds to ligated integrins and terminates the signal to Rho, is discussed in Appendix A.2. Rho inhibition is followed by the disassembly of the stress fibers. Consequently, the decrease in the contractile force slows down the maturation of focal complexes into focal contacts, so the number of focal complexes increases. Simultaneously, Rac is activated because of a positive feedback loop between Rac and focal complexes (see Introduction). When the Rho inhibition recovers, the stress fibers reassemble, generating tension that stimulates the focal complexes maturation into the focal contacts. Consequently, the concentrations of activated Rac and Rho, and the numbers of adhesions and stress fibers return to respective baselines. In the next section, we demonstrate that this model can explain quantitatively the temporal dynamics observed in Tzima et al. (2001, 2002).

2.5. Qualitative model of the cell and stress fibers alignment

2.5.1. How the stress fibers align with each other (Fig. 4)

Based on observations (Zimerman, 2004), we assume that short 'nascent' fibers appear with a constant rate at random locations and angles (Fig. 4A). They shorten and disappear with a small rate (Fig. 4A), and they also translocate. When two such fibers get very close to each other, they 'line-up', meaning that the proximal adhesions at the ends of the fibers merge (Fig. 4B). In the model, we assume that this lining-up process occurs for fibers that meet at an angle, α, that is greater than the right angle. Contractile forces generated by actin–myosin sliding in two nascent fibers pull the merged adhesion between the aligned fibers in almost opposite directions and largely cancel each other. Since adhesions need force for their maintenance (see Introduction), this central adhesion then disassembles, leaving a single fiber oriented at the angle equal to the average orientation of the two initial fibers (Fig. 4B,C). We assume that this fusion process results in either a nascent (Fig. 4B), or a 'mature' (Fig. 4C) fiber. (It would be more accurate to characterize the fibers by the amount of F-actin in the bundle, as well as by their orientation, and introduce the rules for the actin content increase as a result of the fusion, but this would render the mathematical analysis of the model prohibitively complicated.)

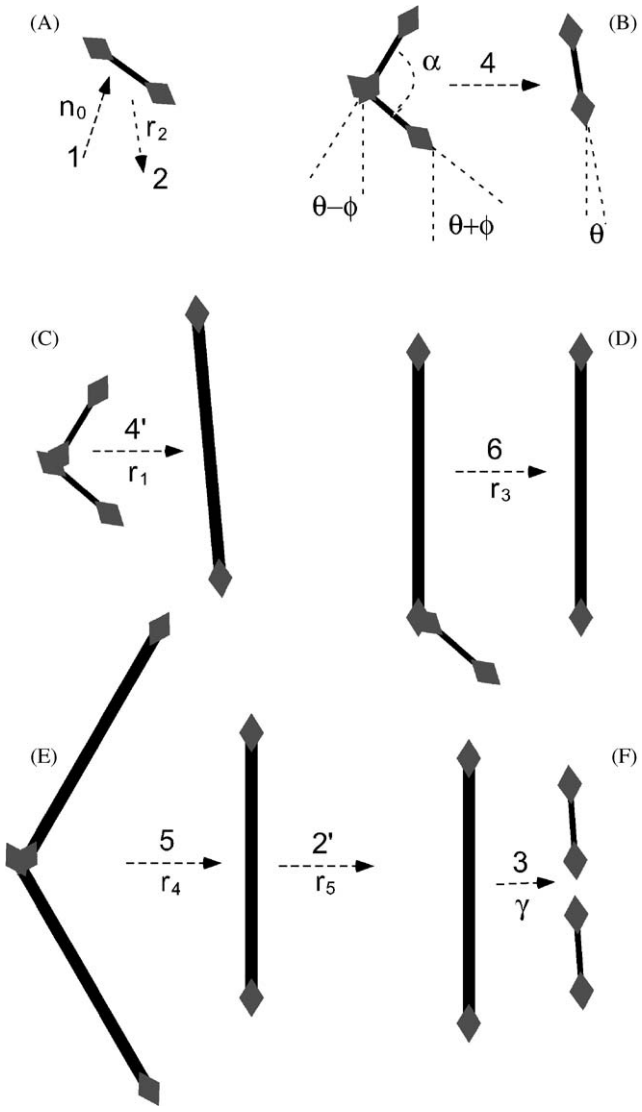

Fig. 4. Schematic illustration of the interactions between stress fibers: the numbers and parameters correspond to the numbers below the terms and under the braces and the reaction rates in the equations (8) and (9). Nascent fibers are short and thin; mature fibers are long and thick; diamonds at the fibers' ends illustrate the adhesions. The nascent fibers nucleate (1), shorten (2), line-up and fuse into nascent (4) or mature (4') fiber. Mature fibers split (3), line up and fuse with each other (5) and line up and fuse with nascent fibers (6).

Similarly, two mature fibers can align and fuse into another mature fiber oriented at the average orientation of the two initial fibers (Fig. 4E). We assume that when a mature and a nascent fibers orient and fuse, a mature fiber with the same orientation as the original mature fiber emerges (Fig. 4D). Finally, mature fibers either shorten and disassemble (Fig. 4E), or shorten or split into the nascent fibers (Fig. 4F).

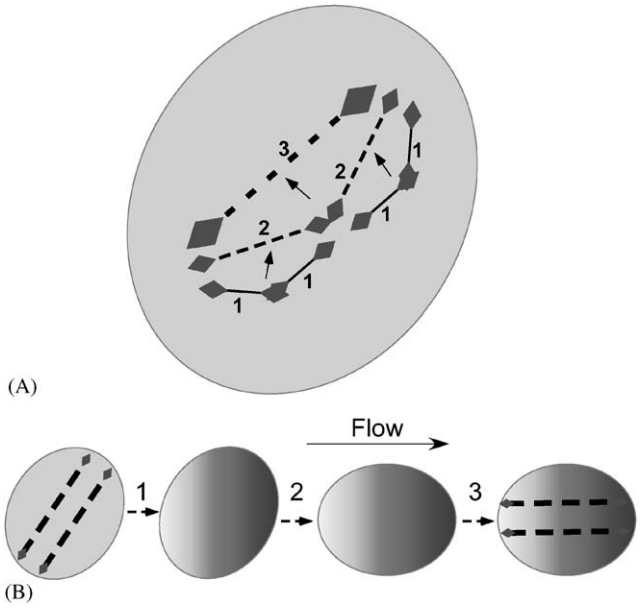

Fig. 5. A. Schematic illustration of the assembly and alignment of stress fibers. Two pairs of the nascent (solid lines, 1) stress fibers (adhesions at their ends are shown with diamonds) line up and fuse. The resulting two fibers (dashed lines, 2) fuse again. Mathematical model demonstrates that, as a result, more thick, long and aligned stress fibers (3) develop. B. The model of cell and fibers alignment: Initially (1), the stress fibers aligned with the long cell axis disassemble and Rac gradient in the direction of the flow develops (shading). Then (2), the cell changes its shape elongating in the direction of the flow. Finally (3), the stress fibers re-assemble along the new cell axis.

Note, that among the described processes, four are lining-up and fusion of the fibers (Fig. 4B–E). As a result of the fusion, fibers emerge at angles that are between the orientation angles of the initial fibers. Effectively, this means that the pairs of fibers align with each other. In Section 6 we will demonstrate that the corresponding mathematical model predicts that if the lining-up and fusion rates are sufficiently high, then a highly aligned distribution of stress fibers evolves (Fig. 5A).

2.5.2. How the stress fibers align with the long axis of the cell

The alignment and fusion processes explain the stress fibers alignment (Fig. 5A), but the isotropy of the described model suggests that the fibers would align along a random direction determined by initial conditions. However, the following additional consideration explains why the fibers align with the long axis of the cell. To account for the effect of the cell shape, note that stress fibers stretching across the whole cell in the direction of its major axis are longer on the average, than stress fibers aligned with the minor axis. Assigning more 'weight' to the long mature stress fibers along the long axis of the cell would make the model effectively anisotropic and explain the stress fiber alignment with the major axis of the cell. Arbitrarily small degree of anisotropy is sufficient to define the predominant alignment direction (Mogilner et al., 1996).

2.5.3. How the cells align with the flow (Fig. 5B)

We suggest the following qualitative model for the initial stage of the cell alignment in the direction of the flow. First, we assume that the presence of the aligned stress fibers prevent the cell shape change. This assumption is based on the analogy of the sheared endothelial cells with motile cells (Davies, 1995): in motile cells containing many stress fibers (i.e. fibroblasts), the boundaries change slowly, while in cells without stress fibers (i.e. keratocytes) the edges move rapidly.

First, the transient decrease in activated Rho causes a drop in myosin dependent contractility that is necessary for the maintenance of the adhesions at the ends of the stress fibers, and therefore leads to the fibers' disassembly. We hypothesize that this 'frees' the cell to change its shape. Second, the transient rise in activated Rac enhances lamellipodial actin network growth at the cell boundary, accelerating the cell shape change. Note, that elevated Rho is generally associated with contractile structures, while elevated Rac corresponds to growing isotropic actin networks (Hall, 1998; Ridley, 2001; Rottner et al., 1999). Crucially, the spatial gradient in the activation of Rac (elevated Rac at the downstream edge of the cell) enhances the lamellipodial growth at the downstream edge of the cell and the ultimate elongation of the cell in the direction of the flow (Fig. 5B).

Finally, recovery of Rho activity in the newly aligned cell causes the re- assembly of the stress fibers and their alignment with the new long axis of the cell. The stress fibers then 'fix' the cell alignment in the direction of the flow (Fig. 5B).

In this paper, we model mathematically only the temporal response of the cell to shear flow and the self-alignment of the stress fibers. More complex processes of cell shape change, its interaction with the stress fiber dynamics and the nature of the Rac gradient are not modeled quantitatively due to lack of experimental data that is needed to derive a corresponding explicit model. In Appendix A.3 we discuss possible physico-chemical mechanisms that could explain qualitatively the spatial gradient in the activation of Rac. Also, we only model the initial two hours of the response during which the cells start to change shape and align with the flow direction. The subsequent elongation and alignment of the cells is likely to depend on microtubules and cell–cell interactions, thus could be much more complex than the processes that we examine here.

3. Mathematical model of the temporal response

3.1. Positive feedback loop between focal complexes and Rac

We describe the system with time dependent densities of Rac, $r(t)$, and Rho, $\rho(t)$, and numbers of the stress fibers, $s(t)$, focal complexes, $c(t)$, and focal contacts, $f(t)$. The model variables are listed in Table 2. Alternatively, function $s(t)$ can have the meaning of the total amount of F-actin or myosin in the stress fibers, and functions $c(t)$, $f(t)$ can mean either the number of integrins in, or the adhesion area of the focal complexes and contacts, respectively. Following the qualitative model, we assume that the rate of Rac activation is an increasing function of the number of the focal complexes, and, in turn, the number of the focal complexes is an increasing function of the Rac concentration. This is depicted by the last terms in the right-hand sides of the following equations:

$$\frac{dr}{dt} = -b_1 r + b_2 c, \quad \frac{dc}{dt} = h(c,\ldots) + b_3 r. \tag{1}$$

The corresponding terms can be nonlinear, for example, Hill functions of the corresponding concentrations, if there are any cooperativity effects in the respective pathways (Edelstein-Keshet, 1988). In the absence of information about the detailed kinetics of these pathways, we choose the linear terms above assuming a Michaelis–Menten type reaction of Rac activation by the focal complexes such that the focal complex is an enzyme, and Rac is a saturated substratum. We assume a similar influence of Rac on the focal complexes. Coefficients b_2 and b_3 are the respective proportionality constants. The first term in the first equation in (1) is responsible for the deactivation of Rac with constant rate b_1. The first term in the second equation in (1) describes the Rac-independent part of the dynamics of focal complexes as explained below. There are no relevant rate measurements available, but the following general considerations suggest a useful time scale separation. Rac activation is likely to be limited by nucleotide exchange and translocation of the small G-protein to the appropriate cellular compartment(s) (Ridley, 2001). The corresponding time scales are likely to be in the range of seconds. On the other hand, the effect of Rac on focal complex assembly is likely to involve intermediate actin scaffold assembly triggered by Rac (Geiger and Bershadsky, 2001). Such processes of F-actin remodeling take place on time scales in the order of 10 min (McGrath et al., 1998). Similarly, de-activation of Rac is likely to occur in seconds, while the focal complex dynamics is much slower. Therefore, we assume that b_1, b_2 are much greater than b_3 and $h(\cdot)$ and that the concentration of Rac is always in a quasi-stationary state determined by the 'slowly' changing number of focal complexes. Mathematically, this means that $dr/dt \approx 0$, and:

$$r \approx \frac{b_2}{b_1} c, \quad k_5 = \frac{b_2 b_3}{b_1}, \quad \frac{dc}{dt} \approx h(c,\ldots) + k_5 c. \tag{2}$$

Therefore, we do not have to solve the equation for Rac concentration explicitly. Rac concentration simply follows linearly the focal complex number. These arguments can be made rigorously using singular perturbation analysis.

Table 2
Temporal model variables

Symbol	Meaning	Units
t	time	min
$i(t)$	ligated signaling integrins	μM
$\rho(t)$	activated Rho	μM
$r(t)$	activated Rac	μM
$c(t)$	focal complexes	μM
$f(t)$	focal contacts	μM
$s(t)$	stress fibers	dimensionless density

3.2. Dynamical system of interacting adhesions, stress fibers, Rac and Rho

The model is described by the following five equations:

$$\frac{di}{dt} = -k_1 g(s) i, \tag{3}$$

$$g(s) = \frac{1}{2}(1 + sign(s_0 - s)),$$

$$\frac{d\rho}{dt} = k_2(1 - k_3 i - \rho), \tag{4}$$

$$\frac{dc}{dt} = k_4(1 - sc) + k_5 c, \tag{5}$$

$$\frac{df}{dt} = k_4(sc - f), \tag{6}$$

$$\frac{ds}{dt} = k_6(\rho - s). \tag{7}$$

Eq. (3) is responsible for the decay of the ligated integrin signaling with the rate k_1. Integrin activation and ligation is assumed to be fast and upstream of the explicitly modeled processes, so $i(0) = 1$: all dependent model variables are introduced in the non-dimensional form. The initial ligated integrin concentration is normalized to 1. We assume that the signaling decay is triggered by the changed intracellular tension. Function $g(s)$ is responsible for mathematical description of this effect: the tension is generated by the stress fibers, so we assume that the signal decays if the number of the stress fibers is below the threshold level s_0. Eq. (4) describes the dynamics of Rho activation, where k_2 is the rate of Rho

de-activation. Stationary Rho concentration is normalized to 1 in the absence of the ligated integrin inhibitory signaling. The inhibition of Rho activation by the signaling ligated integrins is described by the phenomenological linear term $(-k_3 i)$, where k_3 is the proportionality coefficient. The last term in Eq. (5) is described in Section 3.1. The nondimensional focal complex number is normalized to 1 in the absence of the effect from Rac. Parameter k_4 is the rate of focal complex maturation. Based on the results in Riveline et al. (2001), we assume that the maturation rate of the focal complexes into firmer focal contacts is proportional to tensile force, which, in turn, is proportional to the number of the stress fibers. Hence, the maturation rate is proportional to $s(t)$. Eq. (6) has the same term $k_4 sc$, as Eq. (5), but with opposite sign meaning the rate of increase of the focal contact number due to the focal complex maturation. The last term in Eq. (6) describes the disassembly of the focal contacts, such that the steady state number of focal contacts is normalized to 1 at unit values of the focal complex and stress fibers. Finally, Eq. (7) is responsible for the stress fiber disassembly with the rate k_6 and for their assembly proportional to the activated Rho concentration. The assembly term is due to Rho activation of myosin action, which, as discussed in the Introduction, in turn pulls F-actin together into the contractile bundles. In the absence of the quantitative data about the concentration dependencies of this pathway, we introduce the corresponding phenomenological linear term.

The model (3–7) contains seven parameters $k_1 - k_6$ and s_0 (Table 4). The values of these parameters are not known directly from experiments, therefore we use the following arguments based indirectly on available literature to estimate their orders of magnitude. Thus, only the orders of magnitude of the model parameters are justified; their exact values are chosen to fit the experimental results of (Tzima et al. 2001, 2002). The time scale for decay of ligated integrin signal is tens of minutes (Tzima, 2001), so we choose $k_1 = 0.05$/min. Level of activated Rho responds to the ligated integrin signaling in minutes (Tzima et al., 2001), and we choose the corresponding rate $k_2 = 0.5$/min. Up to 50% of Rho is inhibited by the ligated integrin signaling (Tzima et al., 2001), hence the value $k_3 = 0.5$. Many indirect observations scattered throughout the literature indicate that adhesions turn over on the scale of a few minutes (Davies et al., 1994; Zimerman, 2004), so we choose $k_4 = 0.1$/min. Similarly, actin structures turn over in up to 10 min (McGrath et al., 1998), hence $k_6 = 0.1$/min. Assuming that the effect of Rac on focal complexes involves slow, tens of minutes long assembly of actin scaffolds, we choose the corresponding rate $k_5 = 0.02$/min. We assume that a very small change in tension (stress fiber number), on the order of a few percent, blocks the ligated integrin signaling, so $s_0 = 0.95$.

4. Mathematical model of stress fibers alignment

The transient changes in Rho regulate the re-modeling of the stress fibers' angular distribution. A qualitative model of this process is described in Section 2. Here we introduce a mathematical model of stress fiber alignment with each other and with the long axis of the cell. Endothelial cells are polygonal and can be roughly approximated by ellipsoidal shapes. Cell size (the lengths of the ellipse's major and minor axes) is a few tens of microns, while cell thickness (from basal to luminal surface) is but a few microns (Davies et al., 1997), so we choose a flat, 2-D, ellipsoidal cell domain in our model. In this paper we do not attempt to model the spatial structure of the cytoskeleton. It is the angular order that is the object of our investigation here, so we quantify the actin stress fibres with *angular densities of F-actin contained in the nascent and mature fibres*, $n(\theta, t)$ and $m(\theta, t)$, respectively (Table 3). $\theta = 0$ corresponds to the direction of the major (long) cell axis, and $-\pi/2 \leqslant \theta < \pi/2$: the stress fibres are bi-polar bundles, they do not have 'plus' and 'minus' ends, and therefore orientations θ and $\theta + \pi$ correspond to the same fiber.

The following equations based on the qualitative model of Section 2 describe the angular dynamics of the stress fiber distribution:

$$\underbrace{\frac{\partial n}{\partial t}(\theta,t)}_{\text{density change}} = \underbrace{-\frac{1}{2}(I*n)n(\theta,t) + (1-r_1)(n*n)(\theta,t)}_{\text{4: nascent/nascent SF fusion}} + \underbrace{n_0}_{\text{1: nucleation}} - \underbrace{r_2 n(\theta,t)}_{\text{2: shortening}} + \underbrace{\gamma m(\theta,t)}_{\text{3: splitting}} - \underbrace{r_3(I*m)n(\theta,t)}_{\text{6: nascent/mature SF fusion}}, \tag{8}$$

$$\underbrace{\frac{\partial m}{\partial t}(\theta,t)}_{\text{density change}} = \underbrace{r_4\left[-\frac{1}{2}(I*m)m(\theta,t) + (m*m)(\theta,t)\right]}_{\text{5: mature/mature SF fusion}} - \underbrace{r_5 m(\theta,t)}_{\text{2: shortening}} - \underbrace{\gamma m(\theta,t)}_{\text{3: splitting}} + \underbrace{r_1(n*n)(\theta,t)}_{\text{4: nascent/nascent SF fusion}} + \underbrace{r_3(I*n)m(\theta,t)}_{\text{6: nascent/mature SF fusion}}. \tag{9}$$

Table 3
Angular model variables

Symbol	Meaning	Units
t	time	min
θ	angle	rad
$n(\theta, t)$	angular density of nascent stress fibers	1/rad
$m(\theta, t)$	angular density of mature stress fibers	1/rad

The integral terms in these equations have similar form to those in abstract alignment models described and analysed earlier in Geigant et al. (1998) and are defined as follows:

$$(I *_m^n) = \frac{2}{\pi}\int_{-\pi/2\ m}^{\pi/2\ n}(\phi)\,\mathrm{d}\phi, \quad \begin{pmatrix} n & & n \\ & * & \\ m & & m \end{pmatrix}(\theta)$$

$$= \frac{2}{\pi}\int_{-\pi/4\,m}^{\pi/4\,n}(\theta+\phi)\,{}_m^n\,(\theta-\phi)\,\mathrm{d}\phi,$$

The reader is referred to Geigant et al. (1998) for the details of the development of these terms. The meaning of each term on the right-hand side of Eqs. (8) and (9) are given under braces, and the numbers in these descriptions correspond to identically numbered events in Fig. 4. The integral terms $(I * n)$ and $(I * m)$ describe the process of disappearance of a nascent or mature fiber at a given angle as a result of fusion with another fiber at any other angle. The convolution terms $(n * n)(\theta)$ and $(m * m)(\theta)$ describe the emergence of a fiber with orientation θ as a result of the fusion of two fibers with orientations $\theta \pm \phi$, where $-\pi/4 < \phi < \pi/4$. We assume that the fibers line up always in such a way that the angle between them is obtuse (Fig. 4B–E), therefore $-\pi/4 < \phi < \pi/4$. We also assume that the rates of the 'fusion reactions' are proportional to the products of the densities of the fusing fibers by analogy with bi-molecular reaction kinetics. The integral terms are defined in such a way that the amount of F-actin is conserved in the fusion processes. The last term in Eq. (9) accounts for the fusion of mature fibers oriented at θ with a nascent fiber of any orientation. The result is the mature fiber of the original orientation, amount of F-actin in which is increased. The nascent/nascent fusion produces either a nascent, or a mature fiber with relative rates $(1 - r_1)$ and r_1, respectively. The nucleation, shortening and splitting terms are self-explanatory. The model parameters (Tables 4,5) are further discussed in Appendix A.4.

5. Results: Transient dynamics of Rac, Rho, stress fibers and adhesions

As an initial condition, we assume that $i(0) = 1$: the ligated signaling integrins are upstream of all other modeled processes, and their initial number is normalized to 1. When $i = 0$, the steady state solutions of Eqs. (3)–(7) are: $\rho = f = 1, c = f = 1.25$. Assuming that before the onset of shear flow the system is in equilibrium in the absence of the signaling integrins, we use these values as the initial conditions.

We solve Eqs. (3)–(7) numerically using the explicit Euler method (Garcia, 2000). We non-dimensionalize Eqs. (3)–(7) using 10 min as unit of time. Densities of Rac, Rho, stress fibers and focal contacts and complexes are introduced in the non-dimensional form from the beginning. Integration time step is equal to 0.05 time unit. The results of the simulations are shown in Fig. 6.

Table 4
Temporal model parameters

Symbol	Meaning	Value
s_0	threshold stress fibers density	0.95 unit
k_1	rate of ligated integrin signal decay	0.05/min
k_2	rate of Rho de-activation	0.5/min
k_3	integrin/Rho inhibition coefficient	0.5
k_4	rate of focal complex maturation	0.1/min
k_5	effective rate of Rac mediated self-activation of focal complexes	0.02/min
k_6	rate of stress fibers disassembly	0.1/min

Table 5
Angular model parameters

Symbol	Meaning	Value
n_0	stress fiber nucleation rate	0.2
r_1	rate of merging of nascent stress fibers into mature one	0.1
r_2	rate of nascent stress fibers disassembly	0.2
r_3	rate of merging of mature and nascent stress fibers	1
r_4	rate of merging of mature stress fibers	1
r_5	rate of mature stress fibers disassembly	0.1
γ	rate of mature stress fibers fragmentation	0.001

The simulations demonstrate that the level of activated Rho decreases down to half of its initial level in the first 5 min and then adapts to baseline in the next few tens of minutes. The transient decrease in Rho diminishes the rate of stress fibers assembly and the number of the stress fibers decreases. This reduces the tension applied to the adhesions leading to the slowing down of the maturation of the focal complexes into the focal contacts. As a result, the number of the focal complexes (contacts) goes up (down). Note, that because the dynamics of the stress fibers and adhesions is slower than the dynamics of Rho, the transient changes of the adhesions and stress fibers follow the transient Rho decrease with the delay.

After the first 20 min following the onset of the flow, the stress fibers' number starts to increase as Rho activity rebounds. After a small delay, the number of the focal complexes decreases and the number of the focal contacts increases to the respective baselines. Interestingly, the model predicts that the number of the focal

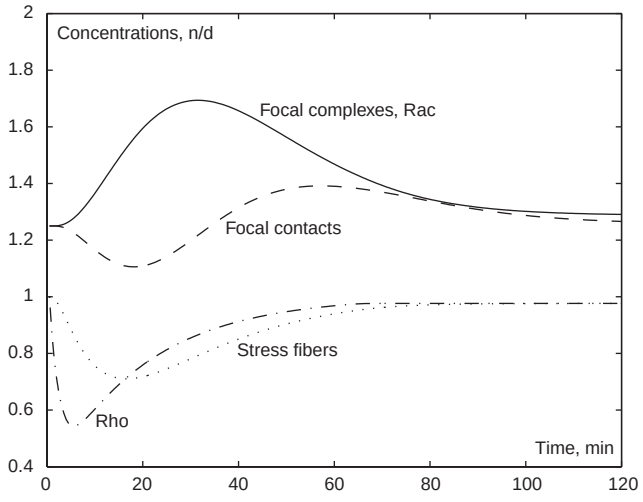

Fig. 6. Numerical solutions of the model equations (3)–(7) for the time dependent non-dimensionalized concentrations and numbers of focal complexes and Rac (solid line), Rho (dot–dashed line), stress fibers (dotted line) and focal contacts (dashed line).

contacts decreases first and then transiently increases above the baseline. This behavior is due to the significant transient increase in the number of the focal complexes so for a period of time the number of maturing adhesions is very large. The transient changes in the system are over by 80–100 min.

The model quantitatively reproduces the observed time courses for Rac and Rho activities and the number of stress fibers described in Section 2. Note that the concentration of Rac in the model is linearly proportional to the number of the focal complexes with the proportionality coefficient unknown and not specified in the model. Therefore, assuming that this coefficient is close to 2, we can explain the observed three-fold increase of Rac 30 min after the flow onset of flow.

The model makes quantitative predictions about the number of adhesions (or the number of integrins in them): a significant transient increase of focal complexes that is maximal at 30 min, a decrease in focal adhesion number by 20 min, followed by an increase to a maximum by 50 min, then decreasing to the baseline.

Existing observations do not allow us to conclude whether the ligated integrin signaling inactivates Rho (which we assumed in the model), or activates Rac and indirectly inhibits Rho through increased focal complexes number, or both. To address this question, we changed the model by introducing the direct activation of Rac by de novo ligated integrins and direct inhibition of Rho by focal complexes. In this case, it is possible by changing the model parameters by less than an order of magnitude to obtain the resulting time courses for the model variables very similar to those of the original model. Thus, without additional data, the model cannot provide an answer to the question about the relative roles of direct integrin signaling and indirect effect of integrins in Rho inactivation and Rac activation.

Finally, we tested the model behavior in the cases where either Rho or Rac is downregulated. In the former case, we decreased to various degrees the first term in the bracket in Eq. (4) making it less than 1. Mathematically, this decreases the equilibrium level of activated Rho without changing its dynamics. As expected, the equilibrium numbers of stress fibers and focal contacts decrease, while the equilibrium number of focal complexes increases. The nontrivial result of the perturbed model simulations is that maximum Rac concentration occurs later than in the unperturbed model. For example, when Rho is downregulated by 50% , the maximum of Rac takes place at 40 min after the flow onset, 10 min later, than in the unperturbed model. On the other hand, downregulation of Rac does not change the transient model behavior, aside from the absolute numbers of adhesions.

6. Results: Alignment of stress fibers

Linear stability analysis of the stress fibers alignment model described in Appendix A.4 gives the result, which is very simple despite the relative complexity of the model: the isotropic stress fibers distribution is unstable when the following inequality is true:

$$\frac{n_0 r_4}{r_5 \gamma} > 3.66. \tag{10}$$

In this case, the angular instability proportional to $\sin(2\theta)$ (more stress fibers in one direction and less in the perpendicular direction) emerges and grows, because the lining up and fusion of the stress fibers leads to effective alignment of the resulting evolving fibers. Inequality (10) has simple meaning: for the angular order, the rate of nucleation of the nascent fibers and the rate of lining up and fusion of mature fibers (processes leading to interactions and angular ordering) have to be great enough, while the rates of shortening, disassembly and splitting of the mature fibers (processes leading to disorder) have to be small enough.

To find the asymptotically stable stationary angular distribution of the stress fibers predicted by the model, we solved Eqs. (8) and (9) numerically. We discretized the interval $-\pi/2 \leqslant \theta \leqslant \pi/2$ (in radians) with the spatial step equal to 0.05 and solved the corresponding system of ODEs using the same method as for the simulation of Eqs. (3)–(7). The integrals in Eqs. (8) and (9) were computed at each time step using Composite Midpoint rule (Garcia, 2000). We used the model parameters listed in Table 5 and discussed in Appendix A.4. We used constant initial conditions perturbed weakly and randomly. The results (stationary distributions evolved after a few time units) are shown in Fig. 7.

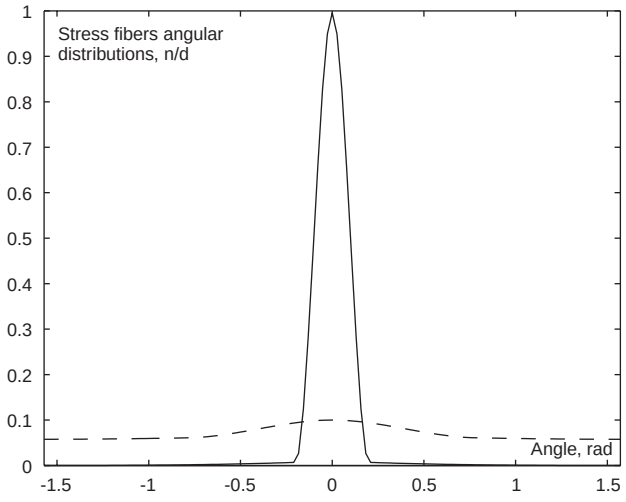

Fig. 7. Numerical solutions of the model equations (8) and (9) showing the asymptotically stable stationary angular densities of the nascent (dashed line) and mature (solid line) stress fibers. The densities are normalized so that the maximal mature fibers density is 1. The respectively scaled nascent fibers density is then multiplied by 20.

The model predicts a very significant alignment of the mature, long stress fibers (they are distributed within a roughly $0.2\,\text{rad} = 10^\circ$ interval). The number of mature stress fibers is an order of magnitude greater than the number of nascent fibers. Also, the nascent fibers are distributed almost isotropically, very weakly aligned with the mature fibers. The reason is that their fast fusion and maturation does not leave them enough time to align significantly.

7. Discussion

In this paper, we propose a quantitative model of the dynamics of actin stress fibers, adhesion sites and Rho GTPases when the cell is exposed to fluid flow. The model does not address the molecular nature of the corresponding mechanosensory response, regulatory pathways or cell mechanics in detail. Instead, we examine the general feedbacks between adhesions, Rac, Rho and actin stress fibers in order to explain the observed dynamics in a quantitative framework. In summary, a diffusive chemical signal triggered by sheared adhesions activates integrins, which then bind ligands and trigger signals that inhibit Rho and possibly activate Rac. We speculate that either change of tension due to stress fibers disassembly or binding of an adaptor molecule to ligated integrins terminates this signal. The transient decrease in activated Rho leads to stress fibers disassembly and slows down the maturation of focal complexes. Return of Rho to baseline leads to the adaptation of the whole system. Activation of Rac is polarized to the downstream edge of the cell. This, together with the diminished number of the stress fibers, allows the change of the cell shapes and their alignment in the direction of the flow. The 'line-up and fusion' processes underlie the stress fibers alignment with each other. Their alignment with the long axis of the cell could be explained by greater amount of F-actin in the longest fibers along the long axes of the cells.

The model supports the view that the cell's machinery responds to the external force as an excitatory system (in dynamical system sense (Edelstein-Keshet, 1988)). Indeed, an external perturbation smaller than a threshold causes only small transient changes in the cell mechanochemistry. On the other hand, one that is greater than the critical force triggers significant transient changes in Rho GTPases' activation levels, adhesion patterns and cytoskeleton. Also, relatively weak external forces trigger internal forces that are order(s) of magnitude greater.

The model successfully reproduces a few semi-quantitative experimental observations (Tzima et al. 2001, 2002), such as (i) the transient decrease of Rho, (ii) the transient increase of Rac, (iii) the transient disassembly of the initial stress fibers and their subsequent reassembly along the flow. In fact, the model results fit the corresponding experimental data for Rac and Rho (Fig. 1B of (Tzima et al., 2002) and Fig. 4B of (Tzima et al., 2001), respectively) quantitatively.

The model also generates a few predictions that could be tested in future experiments. First, the model predicts transient decrease of the number of focal contacts during the first 20 min after the flow onset, followed by a transient increase of this number for the next 40 min, and an eventual adaptation to the baseline level. These transient changes should be slight ($\sim$10% of the baseline value). Second, the number of focal complexes should simply follow the observed changes in Rac. Third, if Rho is downregulated, the maximum during the transient increase of activated Rac concentration should occur later than in the unperturbed case. Fourth, there should be no changes in the transient response if Rac is downregulated. (In this last case we cannot predict the effect of this downregulation on the spatial Rac gradient and its consequences.) Finally, we predict that the rate of fusion of mature stress fibers must be high enough, and the rate of their splitting must be small enough for stress fiber alignment to take place. We also predict that smaller stress fibers are less ordered angularly than the long ones. Detailed quantitative processing of the data similar to that obtained by Zimerman (2004) can test these predictions.

Our model also provides a qualitative understanding of the data of Zhao et al. (1995) on the synergistic effects of fluid shear stress and cyclic stretch on cytoskeletal remodeling in endothelial cells. In their study, Zhao et al. (1995) demonstrate that the stress fibers align perpendicular to the direction of substrate stretch when cells are exposed to cyclic stretch above a threshold level in the absence of fluid flow. They report that alignment

with the flow also occurs in the absence of cyclic stretch when cells are exposed to fluid shear stress above another threshold level. Moreover, they demonstrate that the levels of stress and stretch required for alignment when applied simultaneously, are lower than the corresponding thresholds found for the stress and stretch, when applied separately. Our model explains these results qualitatively as follows. Cyclic stretch physically breaks the stress fibers along the stretch direction, while little affecting the fibers in the perpendicular direction. This effect modifies the angular dependence of the splitting/disassembly terms in Eqs. (8) and (9) in such a way that the rate of splitting/disassembly becomes greater in the direction of stretch, which is the direction normal to flow. As a consequence, the density of evolving stress fibers becomes greater along the flow direction, normal to stretch. The decrease in the threshold levels for shear stress and cyclic stretch, when applied simultaneously, could be simply explained by the increase in the total force, since the forces due to the deformation of substratum and due to shear flow are both applied on the integrins in focal adhesions, and therefore add up. The response is triggered when the weighted sum of the forces exceeds the threshold for adhesion/integrin activation.

More quantitative experimental data on molecular mechanosensory mechanisms, regulatory biochemical pathway and biophysics of the cytoskeletal response are needed to validate the model. The usefulness of the mathematical model, rather speculative in its present form, is that it allows one to examine a few aspects of the cell's response to external forces in a precise quantitative framework.

Acknowledgements

G.C., M.A.S. and A.M. are supported by NIH GLUE grant 'Cell Migration Consortium'. G.C. and A.M. are supported by NSF grant DMS-0073828. I.N. is supported by NIH grants U54 GM64346 and P41 RR13186. J.-J.M. is supported by Swiss National Science Foundation, Grant 31-61716. M.A.S. is supported by NIH grant RO1 HL075092. A.W.O. is supported by AHA fellowship, number 0325654U. We are grateful to B. Geiger for fruitful discussions. A.M. wishes to thank Isaac Newton Institute for Mathematical Sciences where this work was partially done.

Appendix A

A.1. Estimates of relevant forces:

Shear stress that endothelial cells are exposed to in their physiological environment is in the order of $10\,\mathrm{dyn/cm^2}$ corresponding to $1\,\mathrm{pN/\mu m^2}$. The globally stiff endothelial actin meshwork is characterized by an effective Young modulus of $\sim 10\,\mathrm{nN/\mu m^2}$ (Satcher and Dewey, 1996). Thus, shear stress of $1\,\mathrm{pN/\mu m^2}$ cannot deform the actin cytoskeleton significantly. Considering that the characteristic area of the basal surface of a cell is $\sim 10^3\,\mu\mathrm{m}^2$, the total external force on the cell amounts to $\sim 1\,\mathrm{nN}$. The total number of integrins in tens to hundred of focal contacts (hundreds to thousand integrins in each) can be estimated as $\sim 10^4$–10^5, so the *external* force due to physiological levels of shear stress corresponds to ~ 0.01–$0.1\,\mathrm{pN}$ per integrin link. Much stronger *internal* forces are developed in the cell by myosin contraction: cells deform the external surface with forces in the range of 1–$10\,\mathrm{nN/\mu m^2}$ (Galbraith and Sheetz, 1997; Beningo et al., 2001) corresponding to $\sim 1\,\mathrm{pN}$ per integrin link. Also, forces necessary to induce conformational changes in focal adhesions are in the piconewton range per molecule (Jiang et al., 2003). It is likely that the molecules in cell adhesions, pre-stressed by piconewton range forces generated inside the cell by actin–myosin contraction, are near a threshold, and are able to sense an additional external force of ~ 0.01–$0.1\,\mathrm{pN}$, and respond by undergoing a conformational change when the sum of internal and external forces is over the threshold. This sensing process is likely to involve a cooperativity between integrins needed to sense such small force increments (Bruinsma, 2004).

A.2. Adaptor protein terminates the Rho inhibition

One possible mechanism (either alternative, or complementary, to the stress regulated decay of Rho inhibition) is the slow association of an adaptor protein with de novo ligated integrins assuming that the ligated integrin/adaptor protein complex does not signal. We assume that the rate of integrin-adaptor protein association is much slower than the rate of integrin activation and ligation, and therefore, the Rho inhibiting/Rac activating signal grows fast (in minutes) following the onset of the flow and then decays slowly (in tens of minutes). This hypothesis changes the model equations for the ligated integrins as follows. The number of the ligated integrins is governed by the equation:

$$\frac{\mathrm{d}i}{\mathrm{d}t} = h_1(1 - i), \tag{11}$$

where $h_1 \sim 1/\,\mathrm{min}$ is the rate of the integrin ligation. The adaptor/integrin complex, $a(t)$ is assembled at a rate proportional to the number of signaling integrins that are not occupied by the adaptor molecules, $(i - a)$:

$$\frac{\mathrm{d}a}{\mathrm{d}t} = h_2(i - a), \tag{12}$$

where $h_2 \sim 0.05$/min is the corresponding proportionality coefficient.

These two linear equations can be solved analytically:

$$i = 1 - e^{-h_1 t}, \quad a = (1 - e^{-h_2 t}) + \frac{h_2}{h_1 - h_2}(e^{-h_1 t} - e^{-h_2 t}), \tag{13}$$

$$(i - a) = \frac{h_1}{h_1 - h_2}(e^{-h_2 t} - e^{-h_1 t}). \tag{14}$$

As initial conditions, we assume zero concentrations for the ligated integrins and integrin/adaptor complexes at $t = 0$. Following the flow onset, integrins respond to a signal from stressed adhesions and are activated and ligated within a few minutes. The solution (13) and (14) predicts that the ligated integrin concentration increases fast and exponentially to saturation. Growth of the adaptor/integrin complex concentration is limited at first and lags behind the ligated integrin concentration, both because the corresponding binding rate is slower than the rate of integrin ligation, and also because initially there is a low concentration of ligated integrins for the adaptor protein to bind to. However, after a few tens of minutes, the adaptor/integrin complex concentration saturates to the same value as the ligated integrin concentration (on the average, one adaptor molecule is bound to each ligated integrin molecule). The concentration of the *signaling* ligated integrins, which is equal to $(i - a)$ according to the model, increases rapidly in the beginning due to the fast integrin ligation and slow adaptor protein binding to ligated integrins. Then, after a few minutes, this concentration starts to decrease because the ligated integrin concentration saturates while the adaptor/integrin complex concentration continues to grow slowly. This bi-phasic integrin signaling is crucial for the cell's response in the model: a signal from the integrins inhibit Rho briefly and transiently, which triggers significant downstream feedbacks.

A.3. Discussion of the possible mechanism of the polarized Rac activation

There are a few possible physico-chemical mechanisms that could explain qualitatively the spatial gradient in the activation of Rac (elevated Rac at the downstream edge of the cell) reported in Tzima et al. (2002). First, the adhesions at the periphery of the cell are, in general, pulled by myosin contraction towards the cell center. Therefore, the adhesions at the upstream edge of the cell relative to the flow are pulled in the direction of the flow by internal forces so that internal and external forces add. On the other hand, adhesions at the downstream edge of the cell are pulled against the flow by internal forces so that internal and external forces subtract. This mechanical asymmetry could lead to an inhomogeneous chemical signal translating into the gradient in Rac activation. Second, external forces deform integrins directionally, which could be translated into a directional treadmilling of adhesions as a result of a force dependent clustering of integrins preferentially at the downstream edges of focal adhesions and disassembly at their upstream edges (Ballestrem et al., 2001). (Effective movement of adhesions in downstream direction at the onset of the flow was observed (Davies et al., 1994).) As a result, adhesions at the upstream periphery of the cell move away from the cell edge, while adhesions at the downstream cell boundary treadmill towards the cell edge. This asymmetry, coupled to a possible localization of some signaling pathway to the cell periphery, could cause the gradient in Rac activation. Finally, though the cytoskeleton is likely to be very rigid globally, its mechanical properties locally vary a great deal, including domains that are very soft and viscous rather than rigid and elastic (Tseng et al., 2002). Shear stress at the luminal surface is very uneven due to vertical protrusion of the nuclear region (Davies et al., 1994). Tension due to shear stress is larger and the membrane fluidity is higher at the upstream edge of the cell (Fung and Liu, 1993). Because of the soft and viscous cytoskeletal domain, this uneven stress could lead to both a gradient in displacements in the cytoskeleton magnified downstream (reported in Davies et al. (2001) and Helmke et al. (2003)), and a thixotropic flow of the cytoskeleton in the direction of the flow with subsequent alignment and strengthening of the actin network (Jamney, 1991; Satcher and Dewey, 1996). All these biophysical factors can provide an explanation for how the cell senses the direction of the flow.

A.4. Linear stability analysis of the alignment model

It is easy to check by substitution that the isotropic (constant) angular distribution (no angular order) satisfying algebraic equations:

$$-r_1\bar{n}^2 + n_0 - r_2\bar{n} + \gamma\bar{m} - r_3\bar{n}\bar{m} = 0,$$

$$r_1\bar{n}^2 - r_5\bar{m} - \gamma\bar{m} + r_3\bar{n}\bar{m} = 0,$$

is a stationary solution of the model equations (8) and (9). Here $\bar{n}$, $\bar{m}$ are the constant stationary densities of the nascent and mature fibers, respectively.

We choose the model parameter values satisfying the following strong inequalities: $\gamma \ll r_2, r_5$, and $r_1 \ll r_3$. The first one means that the rate of splitting is much less, than the rate of fibers shortening, which seems to be the cases judging from the movies accompanying the paper of Zimerman (2004). The second inequality means that rate of lining up and fusion of two nascent fibers is much slower, than that of nascent and mature fibers. This feature was not quantified in the experiment but can be justified from the geometric consideration: very likely, the limiting step is the alignment process, not the

relatively fast fusion. A long mature fiber has a greater probability of lining up with a nascent fiber than two short fibers with each other, assuming that the alignment starts with translocating the fibers to within close proximity to each other. Two more strong inequalities that we assume are: $n_0 r_3 \gg r_2 r_5$ and $n_0 r_3 \gg r_5^2$ meaning that the nucleation and fusion of nascent fibers is much faster than shortening and disassembly of both nascent and mature fibers. This also seems to be the case based on the movies accompanying the paper of Zimerman (2004). Based on these inequalities, we choose the values of the model parameters listed in Table 5. We choose the parameters in the non-dimensional form from the beginning. We normalize the rate of fusion of the nascent fibers on 1. We assume that the rates of fusion of mature/mature and mature/nascent fibers are the same, but simulations and analysis show that this is not crucial for the results. We choose these rates equal to the rate of fusion of the nascent fibers (equal to 1) and choose all other parameters to satisfy the inequalities discussed above. The model results are robust toward up to a few-fold changes of the parameter values.

Because of the inequalities discussed above, the terms proportional to r_1 and γ in the algebraic equations for constant angular densities can be neglected and the following approximations are valid:

$$n_0 - r_2\bar{n} - r_3\bar{n}\bar{m} \approx 0,$$

$$-r_5\bar{m} + r_3\bar{n}\bar{m} \approx 0.$$

These equations can be easily solved giving the following approximate values for the stationary constant densities:

$$\bar{n} \approx \frac{r_5}{r_3}, \quad \bar{m} \approx \frac{n_0 - (r_2 r_5/r_3)}{r_5} \approx \frac{n_0}{r_5}, \quad \bar{m} \gg \bar{n}.$$

For the used model parameter values used (Table 5), $\bar{m} \approx 2$, $\bar{n} \approx 0.1$. The reason that the number of the mature fibers is much greater than the number of the nascent fibers is that the former disassemble slowly, while the latter fuse relatively rapidly into the mature fibers.

To analyse linear stability of this isotropic steady state, we consider small perturbations in the form:

$$n(\theta, t) = \bar{n} + \tilde{n}(\theta, t), \quad m(\theta, t) = \bar{m} + \tilde{m}(\theta, t),$$

where $\tilde{n} \ll \bar{n}$, $\tilde{m} \ll \bar{m}$, and

$$\int_{-\pi/2}^{\pi/2} \begin{matrix} \tilde{n} \\ \tilde{m} \end{matrix} (\phi)\, \mathrm{d}\phi = 0.$$

(It is easy to demonstrate that in our model the constant stationary angular distribution is stable with respect to small perturbations constant in angular space.) Substituting these expression into Eqs. (8) and (9) and keeping only linear terms with respect to $\tilde{n}, \tilde{m}$, we obtain the linearized model equations:

$$\frac{\partial \tilde{n}}{\partial t} = \bar{n}[-\tilde{n} + (1 - r_1)((1 * \tilde{n}) + (\tilde{n} * 1))] - r_2\tilde{n} + \gamma\tilde{m} - r_3\bar{m}\tilde{n}, \tag{15}$$

$$\frac{\partial \tilde{m}}{\partial t} = r_4\bar{m}[-\tilde{m} + ((1 * \tilde{m}) + (\tilde{m} * 1))] - r_5\tilde{m} - \gamma\tilde{m} + r_1\bar{n}((1 * \tilde{n}) + (\tilde{n} * 1)) + r_3\bar{n}\tilde{m}. \tag{16}$$

The rotational invariance of the model and the fact that reflectional symmetries of Eqs. (8) and (9) are conserved in time (Geigant et al., 1998) imply that, without loss of generality, $\cos(2l\theta), l = 1, 2, 3, \ldots$ (in addition to the constant perturbation characterized by $l = 0$) is a complete orthogonal system of eigenfunctions for the right-hand side of Eqs. (15) and (16).

Substituting the perturbations of the form

$$\begin{matrix} \tilde{n} \\ \tilde{m} \end{matrix} = \begin{matrix} \tilde{n}_l \\ \tilde{m}_l \end{matrix} \exp(\lambda t)\cos(2l\theta),$$

where $\tilde{n}_l(\tilde{m}_l)$ is the nascent (mature) fibers perturbation amplitude, and λ is the linear growth rate, into linearized equations (15) and (16) we obtain the following linear algebraic system of equations for perturbation amplitudes:

$$\lambda\tilde{n}_l = [\bar{n}(-1 + (1 - r_1)K_l) - r_2 - r_3\bar{m}]\tilde{n}_l + \gamma\tilde{m}_l, \tag{17}$$

$$\lambda\tilde{m}_l = r_1\bar{n}K_l\tilde{n}_l + [r_4\bar{m}(-1 + K_l) - r_5 - \gamma + r_3\bar{n}]\tilde{m}_l, \tag{18}$$

$$K_l = \frac{4}{\pi l}\sin\left(\frac{\pi}{2}l\right). \tag{19}$$

Standard analysis (Edelstein-Keshet, 1988) gives the linear growth rates as the eigenvalues of the matrix:

$$\begin{pmatrix} [\bar{n}(-1 + (1 - r_1)K_l) - r_2 - r_3\bar{m}] & \gamma \\ r_1\bar{n}K_l & [r_4\bar{m}(-1 + K_l) - r_5 - \gamma + r_3\bar{n}] \end{pmatrix}.$$

In the relevant range of parameters, $\bar{n} \approx r_5/r_3$, the terms $(-r_5 + r_3\bar{n})$ cancel, and the matrix simplifies to:

$$\begin{pmatrix} [\bar{n}(-1 + (1 - r_1)K_l) - r_2 - r_3\bar{m}] & \gamma \\ r_1\bar{n}K_l & [r_4\bar{m}(-1 + K_l) - \gamma] \end{pmatrix}.$$

It is easy to check that when $l \geqslant 2$, $|K_l| < 1$, the diagonal elements of the matrix are negative, and the matrix's trace is negative, while the matrix's determinant is positive. These are the necessary and sufficient conditions for the real part of the linear growth rate λ to be negative (Edelstein-Keshet, 1988) and for the constant angular distribution to be stable.

However, at $l = 1, K_1 = 4/\pi > 1$, and when parameter r_4 is large enough, while parameter γ is small enough, the lower diagonal element of the matrix becomes

positive. Then, at small enough γ, the determinant of the matrix becomes negative (upper diagonal element is positive, lower diagonal element is negative, and the product of the off-diagonal elements is very small), and the real part of the linear growth rate of one of the perturbations becomes positive (Edelstein-Keshet, 1988). For example, for the values of the model parameters that we use (Table 5), the matrix is approximately equal to

$$\begin{pmatrix} -2.2 & 0.001 \\ 0.012 & 0.54 \end{pmatrix}$$

and the linear growth rate of one of the perturbations is negative (≈ -2.2), while the growth rate of another perturbation is positive (≈ 0.54).

Biologically, the instability in the relevant parameter range is guaranteed if the effective rate of fusion of the mature fibers is greater than their effective rate of splitting. More precisely, when the value of γ is very small, the positivity of the lower diagonal element of the matrix is the sufficient condition of the angular instability and subsequent alignment. Mathematically, this gives inequality (10) as the criterion of alignment.

References

Arthur, W.T., Burridge, K., 2001. RhoA inactivation by p190RhoGAP regulates cell spreading and migration by promoting membrane protrusion and polarity. Mol. Biol. Cell. 12, 2711–2720.

Arthur, W.T., Petch, L.A., Burridge, K., 2000. Integrin engagement suppresses RhoA activity via a c-Src-dependent mechanism. Curr. Biol. 10, 719–722.

Balaban, N.Q., Schwarz, U.S., Riveline, D., Goichberg, P., Tzur, G., Sabanay, I., Mahalu, D., Safran, S., Bershadsky, A., Addadi, L., Geiger, B., 2001. Force and focal adhesion assembly: a close relationship studied using elastic micropatterned substrates. Nat. Cell Biol. 3, 466–472.

Ballestrem, C., Hinz, B., Imhof, B.A., Wehrle-Haller, B., 2001. Marching at the front and dragging behind: differential alphaVbeta3-integrin turnover regulates focal adhesion behavior. J. Cell Biol. 155, 1319–1332.

Beningo, K.A., Dembo, M., Kaverina, I., Small, J.V., Wang, Y.L., 2001. Nascent focal adhesions are responsible for the generation of strong propulsive forces in migrating fibroblasts. J. Cell Biol. 153, 881–888.

Bray, D., 2001. Cell Movements: From Molecules to Motility. Garland Publishing, New York.

Bruinsma, R., 2004. Adhesion-site force regulation and action-reaction paradox. Biophys. J., in press.

Davies, P.F., 1995. Flow-mediated endothelial mechanotransduction. Physiol. Rev. 75, 519–560.

Davies, P.F., Robotewskyj, A., Grien, M.L., 1994. Quantitative studies o endothelial cell adhesion: directional remodeling of focal adhesion sites in response to flow forces. J. Clin. Inv. 93, 2031–2038.

Davies, P.F., Barbee, K.A., Volin, M.V., Robotewskyj, A., Chen, J., Joseph, L., Griem, M.L., Wernick, M.N., Jacobs, E., Polacek, D.C., dePaola, N., Barakat, A.I., 1997. Spatial relationships in early signaling events of flow-mediated endothelial mechanotransduction. Ann. Rev. Physiol. 59, 527–549.

Davies, P.F., Shi, C., DePaola, N., Helmke, B.P., Polacek, D.C., 2001. Hemodynamics and the focal origin of atherosclerosis: a spatial approach to endothelial structure, gene expression and function. Ann. NY Acad. Sci. 947, 7–16.

Edelstein-Keshet, L., 1988. Mathematical Models in Biology. Random House, New York.

Fung, Y.C., Liu, S.Q., 1993. Elementary mechanics of the endothelium of blood vessels. J. Biomech. Eng. 115, 1–12.

Galbraith, C.G., Sheetz, M.P., 1997. A micromachined device provides a new bend on fibroblast traction forces. Proc. Natl Acad. Sci. USA. 94, 9114–9118.

Galbraith, C.G., Skalak, R., Chien, S., 1998. Shear stress induces spatial reorganization of the endothelial cell cytoskeleton. Cell Motil. Cytoskel. 40, 317–330.

Garcia, A.L., 2000. Numerical Methods for Physics. Prentice Hall, Engle-wood Cliffs, NJ.

Geigant, E., Ladizhansky, K., Mogilner, A., 1998. An integro-differential model for orientational distribution of F-actin in cells. SIAM J. Appl. Math. 59, 787–809.

Geiger, B., Bershadsky, A., 2001. Assembly and mechanosensory function of focal contacts. Curr. Opin. Cell Biol. 13, 584–592.

Giancotti, F.G., Ruoslahti, E., 1999. Integrin signaling. Science 285, 1028–1033.

Girard, P.R., Nerem, R.M., 1993. Endothelial cell signaling and cytoskeletal changes in response to shear stress. Front. Med. Biol. Eng. 5, 31–36.

Hall, A., 1998. Rho GTPases and the actin cytoskeleton. Science 279, 509–514.

Helmke, B.P., Rosen, A.B., Davies, P.F., 2003. Mapping mechanical strain of an endogenous cytoskeletal network in living endothelial cells. Biophys. J. 84, 2691–2699.

Ishida, T., Takahashi, M., Corson, M.A., Berk, B.C., 1997. Fluid shear stress-mediated signal transduction: how do endothelial cells transduce mechanical force into biological responses? Ann. NY Acad. Sci. 811, 12–24.

Jamney, P.A., 1991. Mechanical properties of cytoskeletal polymers. Curr. Opin. Cell Biol. 3, 4–11.

Jiang, G., Giannone, G., Critchley, D.R., Fukumoto, E., Sheetz, M.P., 2003. Two-piconewton slip bond between fibronectin and the cytoskeleton depends on talin. Nature 424, 334–337.

Kano, Y., Katoh, K., Fujiwara, K., 2000. Lateral zone of cell-cell adhesion as the major fluid shear stress-related signal transduction site. Circ. Res. 86, 425–433.

Maniotis, A.J., Chen, C.S., Ingber, D.E., 1997. Demonstration of mechanical connections between integrins, cytoskeletal filaments, and nucleoplasm that stabilize nuclear structure. Proc. Natl Acad. Sci. USA 94, 849–854.

Mathur, A.B., Truskey, G.A., Reichert, W.M., 2000. Atomic force and total internal reflection fluorescence microscopy for the study of force transmission in endothelial cells. Biophys. J. 78, 1725–1735.

McGrath, J.L., Tardy, Y., Dewey, C.F., Meister, J.-J., Hartwig, J.H., 1998. Simultaneous measurements of actin filament turnover, filament fraction, and monomer diffusion in endothelial cells. Biophys. J. 75, 2070–2078.

Mogilner, A., Edelstein-Keshet, L., Ermentrout, G.B., 1996. Selecting a common direction. II. Peak-like solutions representing total alignment of cell clusters. J. Math. Biol. 34, 811–842.

Nimnual, A.S., Taylor, L.J., Bar-Sagi, D., 2003. Redox-dependent down-regulation of Rho by Rac. Nat. Cell Biol. 5, 236–241.

Ridley, A.J., 2001. Rho family proteins: coordinating cell responses. Trends Cell Biol. 11, 471–477.

Riveline, D., Zamir, E., Balaban, N.Q., Schwarz, U.S., Ishizaki, T., Narumiya, S., Kam, Z., Geiger, B., Bershadsky, A.D., 2001. Focal contacts as mechanosensors: externally applied local mechanical force induces growth of focal contacts by an mDia1-dependent and ROCK-independent mechanism. J. Cell Biol. 153, 1175–1186.

Rottner, K., Hall, A., Small, J.V., 1999. Interplay between Rac and Rho in the control of substrate contact dynamics. Curr. Biol. 9, 640–648.

Satcher, R.L., Dewey, C.F., 1996. Theoretical estimates of mechanical properties of the endothelial cell cytoskeleton. Biophys. J. 71, 109–118.

Sawada, Y., Sheetz, M.P., 2002. Force transduction by Triton cytoskeletons. J. Cell Biol. 2002 156, 609–615.

Schoenwaelder, S.M., Burridge, K., 1999. Bidirectional signaling between the cytoskeleton and integrins. Curr. Opin. Cell Biol. 11, 274–286.

Schwartz, M.A., Shattil, S.J., 2000. Signaling networks linking integrins and rho family GTPases. Trends Biochem. Sci. 25, 388–391.

Sherratt, J.A., Lewis, J., 1993. Stress-induced alignment of actin filaments and the mechanics of cytogel. Bull. Math. Biol. 55, 637–654.

Suciu, A., Civelekoglu, G., Tardy, Y., Meister, J.-J., 1997. Model for the alignment of actin filaments in endothelial cells subjected to fluid shear stress. Bull. Math. Biol. 59, 1029–1046.

Tseng, Y., Kole, T.P., Wirtz, D., 2002. Micromechanical mapping of live cells by multiple-particle-tracking microrheology. Biophys. J. 83, 3162–3176.

Tzima, E., del Pozo, M.A., Shattil, S.J., Chien, S., Schwarz, M.A., 2001. Activation of integrins in endothelial cells by fluid shear stress mediates Rho-dependent cytoskeletal alignment. EMBO J. 20, 4639–4647.

Tzima, E., del Pozo, M.A., Kiosses, W.B., Mohamed, S.A., Li, S., Chien, S., Schwarz, M.A., 2002. Activation of Rac by shear stress in endothelial cells mediates both cytoskeletal reorganization and effects on gene expression. EMBO J. 21, 6791–6800.

Van Leeuwen, F.N., Olivo, C., Grivell, S., Giepmans, B.N., Collard, J.G., Moolenaar, W.H., 2003. Rac activation by lysophosphatidic acid LPA1 receptors through the guanine nucleotide exchange factor Tiam1. J. Biol. Chem. 278, 400–406.

von Wichert, G., Jiang, G., Kostic, A., De Vos, K., Sap, J., Sheetz, M.P., 2003. RPTP-alpha acts as a transducer of mechanical force on alphav/beta3-integrin-cytoskeleton linkages. J. Cell Biol. 161, 143–153.

Wang, N., Butler, J.P., Ingber, D.E., 1993. Mechanotransduction across the cell surface and through the cytoskeleton. Science 260, 1124–1127.

Webb, D.J., Parsons, J.T., Horwitz, A.F., 2002. Adhesion assembly, disassembly and turnover in migrating cells—over and over and over again. Nat. Cell Biol. 4, E97–E100.

Zamir, E., Geiger, B., 2001. Molecular complexity and dynamics of cell-matrix adhesions. J. Cell Science 114, 3583–3590.

Zamir, E., Katz, M., Posen, Y., Erez, N., Yamada, K.M., Katz, B.Z., Lin, S., Lin, D.C., Bershadsky, A., Kam, Z., Geiger, B., 2000. Dynamics and segregation of cell-matrix adhesions in cultured fibroblasts. Nat. Cell Biol. 2, 191–196.

Zhao, S., Suciu, A., Ziegler, T., Moore Jr., J.E., Burki, E., Meister, J.J., Brunner, H.R., 1995. Synergistic effects of fluid shear stress and cyclic circumferential stretch on vascular endothelial cell morphology and cytoskeleton. Arterioscler. Thromb. Vasc. Biol. 15, 1781–1786.

Zimerman, B., Volberg, T., Geiger, B., 2004. Early molecular events in the assembly of the focal adhesion-stress fiber complex during fibroblast spreading. Cell Motil. Cytoskel. 58, 143–159.